Annals of Biomedical Engineering, Vol. 25, pp. 180–189, 1997
Printed in the USA.

0090-6964/97 $10.50 + .00

A Quantitative Assay for Intercellular Aggregation

SRIRAM NEELAMEGHAM*† and KYRIACOS ZYGOURAKIS*

*Department of Chemical Engineering and the Institute of Biosciences and Bioengineering, Rice University, Houston, TX, and
†Section of Leukocyte Biology, Department of Pediatrics, Baylor College of Medicine, Houston, TX

Abstract—In an earlier communication (Munn *et al.*, J Immunol. Methods 166:11–25, 1993), we presented the initial development of a quantitative assay for monitoring the rates of cellular aggregation based on digital image processing and video microscopy. This study describes some important enhancements and modifications to the procedure. A new index is introduced to characterize the three-dimensional morphology of the aggregates. This index is based on temporal changes in the projected area of the cells and cell aggregates during the course of the experiment. By drawing an analogy with the kinetic theory of gases, we have also introduced a procedure to normalize for variations in cell seeding density among different experiments. In addition, the image analysis technique has been improved by introducing a background subtraction algorithm to remove illumination defects and an adaptive segmentation procedure. These improvements allowed us to completely automate the image analysis procedure, thus minimizing user intervention and improving the reproducibility of the measurements. The enhanced visual assay is evaluated using some recent results from our studies on homotypic lymphocyte aggregation.

Keywords—Adhesion, Homotypic, Lymphocyte, β_1-Integrin, Digital image analysis, Video microscopy.

INTRODUCTION

Lymphocyte adhesion is an important event during immune response, and it is necessary to understand the pathways of adhesion processes before we can devise strategies to control human immune response (8,9,17). One way to study the adhesion of lymphocytes is to activate them by adding antibodies to certain integrin proteins and then allowing them to aggregate homotypically (2,16). This is one of the experimental approaches we are using in our effort to elucidate the role of anti-β_1-antibodies (against very late activation (VLA) integrins) in lymphocyte adhesion.

A quantitative assay is necessary to explore the pathways in homotypic lymphocyte aggregation and to identify the governing parameters. Several techniques have been previously used to follow the kinetics of aggregation under flow conditions (4,10,12,15,18,19). Such assays, however, may effect the aggregates in an unpredictable manner due to the excess shearing and rupturing of larger aggregates (for some experimental setups, at least). Also, the adhesion of many cells cannot be studied in a shear field, because long contact times are required to form cell–cell bonds. For example, studies in our laboratory have shown that Jurkat cells activated by antibodies to the β_1-integrin do not form homotypic aggregates when exposed to shear in a test tube with a magnetic stir bar.

To alleviate these problems, homotypic cell aggregation is studied under optical microscopes without any flow effects. The traditional visual assays are either qualitative or semiquantitative at best (6,16). Although these methods are adequate for detecting large differences in the extent of aggregation between various systems, they are unable to make more subtle comparisons about the three-dimensional structure and size distribution of aggregates. They also do not provide any information on the kinetics of aggregation, information that is often needed to make deductions about the activation pathway involved. To overcome these problems, we have recently developed a novel visual assay of cell aggregation based on time-resolved morphological measurements that are obtained with image analysis techniques (13).

In the current study, we present some significant enhancements and modifications to this assay. We introduce a new index to characterize the three-dimensional morphology of the aggregates and a method to normalize for differences in cell seeding density among different experiments. Significant enhancements to the image processing techniques are also introduced. These include procedures to (a) enhance the spatial resolution and accuracy of measurements, (b) correct image defects due to uneven illumination, and (c) perform adaptive segmentation of the digital images. These improvements allow us to automate further the image processing and data analysis steps to minimize user intervention and to improve the reproducibility of the measurements. We will describe the enhanced visual assay using some recent results from our studies on the mechanism of aggregation induced by antibodies to the β_1-integrin (14).

Acknowledgment—The 33B6 antibody is a generous gift from Dr. B. W. McIntyre (M.D. Anderson Cancer Center, Houston, TX).

Address correspondence to Kyriacos Zygourakis, Department of Chemical Engineering, MS 362, Rice University, P.O. Box 1892, Houston, TX 77251-1892, U.S.A.

(Received 15Feb96, Accepted 10Apr96)

CELL CULTURE MATERIALS AND METHODS

The examples discussed in this study involve the homotypic aggregation of Jurkat cells (a human lymphoblastoid T cell line). These cells aggregate when monoclonal antibody (mAb) 33B6, an antibody to the β_1-integrin, is added to the culture media in its ascites form. Bednarczyk *et al.* (3) have shown that the 33B6 mAb activates lymphocytes and induces vigorous homotypic aggregation under normal physiological conditions of 37°C and neutral pH. Activation of cells by anti-β_1-antibodies is epitope specific, but isotype and Fc independent (5). It requires an active metabolism, cytoskeletal integrity, physiological levels of intracellular calcium, and functional Na^+/H^+ antiport (1,20). The control antibody used herein is OKT11 that attaches to the CD2 receptor, but does not induce aggregation of Jurkat cells beyond the levels of spontaneous aggregation observed when no antibody is added to the culture media.

Jurkat cells are maintained in RPMI-1640 (Sigma Chemical Co., St. Louis, MO, U.S.A.) supplemented with 10% fetal bovine serum (Sigma). For our experiments, the cells are washed and suspensions are prepared with a concentration of 5.4×10^5 cells ml^{-1} using a hemocytometer. Cells are then activated with mAbs to the β_1-integrin and 100 µl of the activated cell suspension is pipetted into each well of a 96-well tissue culture treated plate (Corning Glass Works, Corning, NY, U.S.A.). This corresponds to a cell seeding density of 1,700 cells mm^{-2}. Cells are allowed to settle and adhere to the bottom of the well at room temperature for 30 min before being placed in a microincubator and transferred to the stage of an inverted optical microscope. We observed some unavoidable variations in the cell seeding densities between the various sections of the well (±200 cells/mm^2). A simple technique to account for the effect of cell density variations on aggregation kinetics is presented in the Appendix.

VISUAL AGGREGATION ASSAY

Videomicroscopy Apparatus

An experimental setup has been developed to automate the image acquisition steps and to control the environment of the microincubator at normal physiological levels as described earlier (13). Briefly, the microincubator containing the 96-well tissue culture plate is mounted on the motorized state (MAC 2000, LEP Limited, Hawthorne, NY, U.S.A.) of an inverted light microscope (Sedival aus-Jena, Seiler Instruments, St. Louis, MO, U.S.A.). The microincubator is maintained at 37°C (±0.1°C) under flowing humidified air with 5% CO_2. Water up to a height of 6 mm is added to the microincubator to increase its heat capacity and thus reduce the temperature sensitivity and thermal gradients within the system. The added water also keeps the atmosphere in the microincubator saturated with water vapor and minimizes media evaporation.

AT 30-min intervals during the experiment, the motorized stage is moved under computer control to capture a mosaic of four adjacent images (640×480 pixels each, 256 gray levels; 1 pixel = 1.258 µm) from each monitored well (Fig. 1a). The four digital images are then processed, segmented, and combined to form a large composite image ($1{,}280 \times 960$ pixels) as shown in Fig. 1b. By capturing the image of a large area without decreasing the magnification of the microscope objective, we improve the spatial resolution of our assay and increase the number of cell aggregates captured and analyzed. This improves the statistics and reduces the reproducibility error.

Image Processing Steps

The activated Jurkat cells and cell aggregates migrate on the surface of the tissue culture plate and collide with other cells and cell aggregates. The colliding species adhere to each other and form larger cell aggregates. A sequences of composite digital images is acquired at fixed time intervals (typically every 30 min for 8 to 10 hr after activation) to monitor the kinetics of the aggregation process. An automated image processing program is then run on all the images to segment these images, identify the aggregates, and obtain their statistics.

The original images suffer from defects like nonuniform illumination and noise. To correct these problems and to improve the aggregate measurements, we have developed a variant of the public domain NIH-Image image analysis software (National Institutes of Health, available via anonymous ftp from zippy.nimh.nih.gov). This variant implements a new background subtraction routine that uses a gray-level interpolation technique (7). First, the original image is divided into small rectangles of size 96×64 pixels, and the modal gray-level value in each rectangle is calculated. Then, a new background image equal in size to the original image is created by (a) setting the pixel at the center of each rectangle to the modal gray-level value computed in the previous step and (b) setting the remaining pixels using cubic spline interpolation. The background image constructed in this fashion has the characteristics of the original's background. The new background image is scaled and subtracted from the original to get a uniformly illuminated image. The noise from this modified image is removed by applying a smoothing filter that uses a simple 3×3 kernel with unit coefficients.

The next step involves segmenting the processed image using a threshold. In the resulting binary image, the cells appear in black while the background is white. The thresholding procedure has been automated using an adaptive

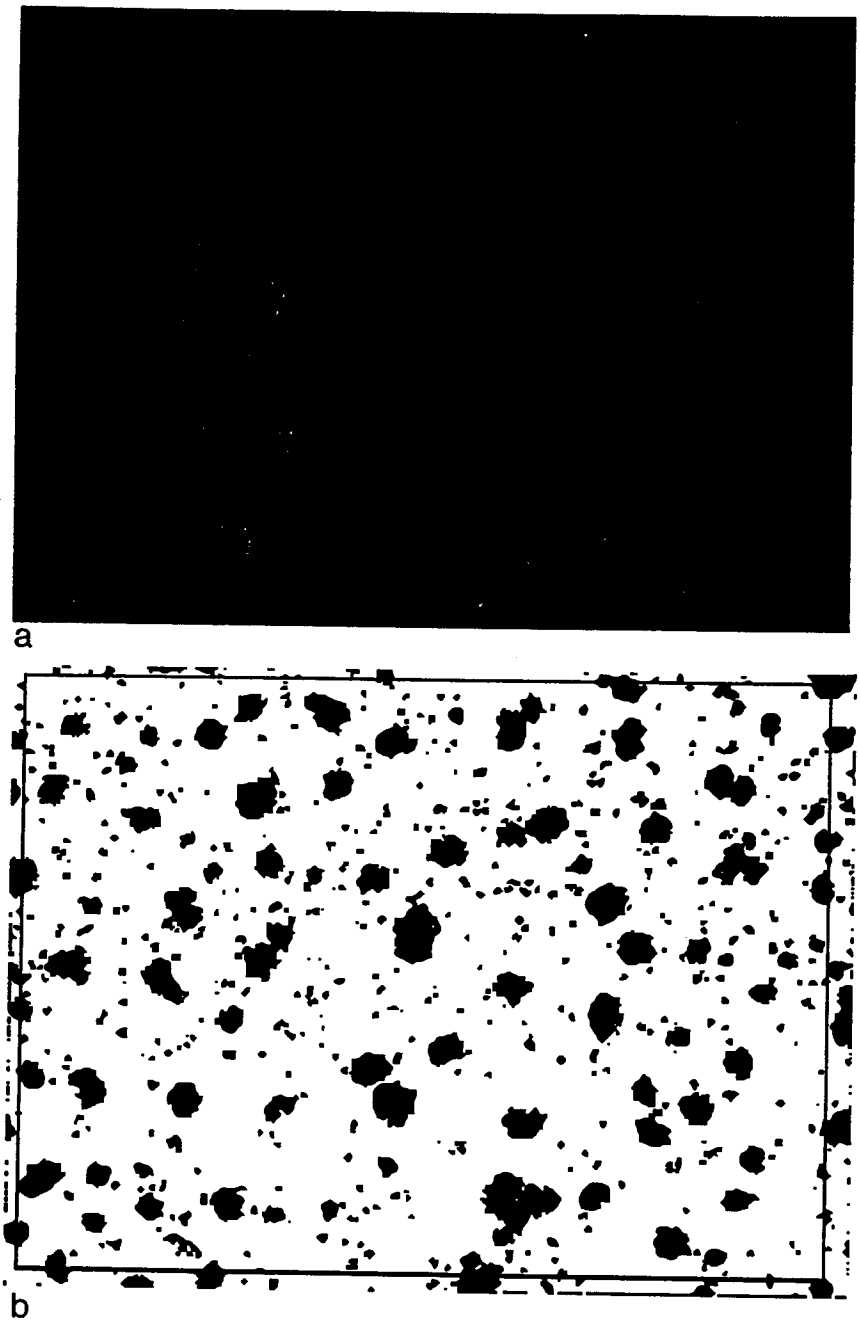

FIGURE 1. Composite image of monitored area of aggregation. (a) At 30-min intervals during an aggregation experiment, the motorized stage is moved under computer control to capture a mosaic of four adjacent digital images (640 x 480 pixels, 256 gray levels) from each monitored well. (b) The four images are later processed, segmented, and combined to form a large composite image (1,280 x 960, binary image). A rectangular region of interest is defined inside the composite image (see text), and only the objects inside it are analyzed to identify single cells and cell aggregates (black objects).

technique based on the gray-scale histogram of each image. Histograms from all our images show two peaks (13). The peak located at low gray-level values contains the information of the background, whereas the peak located at high gray-level values is associated with the pixels belonging to the cells and cell aggregates. To isolate the cell aggregates, the image must be segmented using a threshold located between these two peaks. If M is the gray level corresponding to the minimum between the two peaks and $H(M)$ is the frequency of gray-level M, the threshold gray-level T is chosen such that its frequency $H(T)$ satisfies the equation

$$H(T) - H(M) = K \qquad \text{where} \quad T < M. \qquad (1)$$

The choice of segmentation constant, K, on the right-hand side of Eq. 1 depends on the illumination and the cell type being studied. For all of the systems that we have examined in our laboratory, a K value of 200 provided satisfactory image segmentation. Equation 1 is automatically applied to all images and segmentation proceeds without

user intervention. Although Eq. 1 is empirical, it gives satisfactory and well-reproducible results for all of the aggregation systems we have investigated. Aggregate statistics showed very small differences when measurements obtained with the automatic segmentation procedure were compared with measurements obtained for the same experiment with an operator-selected threshold.

The binary image obtained by thresholding the processed gray-level image is then refined by a series of erosion and dilation operations. Erosion smoothes the contours of the image and eliminates single-pixel noise that may be present in the image. Dilations, on the other hand, fuse narrow breaks in the aggregates, and close holes and gaps in the objects. After this, the four adjacent images are combined to get a composite image with 1,280 × 960 pixels (Fig. 1b), and the projected areas of the identified objects (aggregates and single cells) are calculated.

Errors in the morphological measurements will be introduced if aggregates that touch the edges of the image are included in our calculations. To avoid such errors, we define a rectangular region of interest inside the composite image. Only those aggregates whose centroids are located within this region are used for our measurements (Fig. 1b). The edges of this rectangle are defined by identifying the centroids of the largest objects (aggregates) touching each of the four edges of our composite binary image.

AGGREGATION SIZE AND MORPHOLOGY INDICES

At the start of an aggregation experiment, cells are mainly found as singlets along with some doublets and a few small aggregates. There are no three-dimensional clumps at this point, and all the cells touch the surface of the well. Let M_0 be the total number of objects (aggregates and nonaggregated cells) identified at $t = 0$, and let $A_j(0)$, $j = 1, 2, \ldots, M_0$ be the projected areas of these objects. The initial number of cells N_0 for an experiment can then be calculated by

$$N_0 = \frac{S_0}{a_1} = \frac{\sum_{j=1}^{M_0} A_j(0)}{a_1}, \tag{2}$$

where S_0 is the total initial projected area of all the cells, and a_1 is the area of a single cell. If we assume that the cells do not divide during the course of the experiment (a valid assumption for our lymphocyte system), the total number of cells computed herein remain constant and equal to N_0.

As aggregation proceeds, single cells (singlets) and small aggregates continuously combine to form larger aggregates. Therefore, the total number of objects (aggregates and singlets) identified by our image analysis procedure decreases with time, whereas their average size increases. In general, however, aggregates have a three-dimensional structure with many cells stacked on top of each other. Cells incorporated in three-dimensional aggregates can be classified in two categories: (a) those located at the base of the aggregates (and therefore touching the surface of the tissue culture plate) and (b) those stacked on top of other cells (and therefore not in contact with the well bottom).

At any time t after the start of the experiment, let $M(t)$ be the total number of objects (aggregates and nonaggregated cells) and let $A_j(t)$, $j = 1, 2, \ldots, M(t)$ be the projected areas of the objects on the focal plane (*i.e.*, the well bottom). The number $N_{bj}(t)$ of cells located at the base of a three-dimensional aggregate can be computed from the projected area $A_j(t)$ as follows:

$$N_{bj}(t) = \frac{A_j(t)}{a_1}. \tag{3}$$

To determine the total number $N_s(t)$ of cells stacked on top of the cells forming the base of the three-dimensional aggregates, we first calculate the total projected area $S(t)$ of all the objects:

$$S(t) = \sum_{j=1}^{M(t)} A_j(t). \tag{4}$$

The total projected area $S(t)$ decreases with time as the aggregating cells stack on top of each other to form multilayered clumps. The net decrease of the total area can be used to calculate the total number of stacked cells, $N_s(t)$:

$$N_s(t) = \frac{S_0 - S(t)}{a_1}. \tag{5}$$

The stacked cells $N_s(t)$ must then be distributed among the three-dimensional aggregates. Because only aggregates consisting of more than three cells exhibit three-dimensional stacking, $N_s(t)$ must be distributed over aggregates with a projected area $A_j(t)$ greater than $3a_1$. One approach for distributing the stacked cells is to make assumptions about the aggregate shape. If the aggregates are assumed to be hemispherical, for example, the number of cells $N_{sj}(t)$ located above the focal plane (*i.e.*, stacked on other cells) of an aggregate with a projected area of $A_j(t)$ is

$$N_{sj}(t) = \frac{1}{2}\left(\frac{A_j(t)}{a_1}\right)^{3/2} - \frac{A_j(t)}{a_1}. \tag{6}$$

This approach does not necessarily conserve the total number of cells, and any deviations of actual aggregate shapes from perfect hemispheres will lead to erroneous estimates of aggregate sizes. The total number of cells is conserved, however, when the following empirical equa-

tion is used to distribute the stacked cells among the different aggregates:

$$N_{sf}(t) = \left(\frac{((A_f(t))^n}{\sum_{A_i(t)>3a_1} A_1(t)^n}\right)\left(\frac{S_0 - S(t)}{a_1}\right). \quad (7)$$

The exponent n must be assigned a value between 1 and 3/2, depending on the shape of the three-dimensional aggregate. If n is set equal to 1, the stacked cells $N_s(t)$ are distributed in proportion to the projected areas of the individual aggregates. This is usually a good starting value for n and is applicable for aggregates that are relatively flat with limited vertical stacking. If, on the other hand, experimental observations reveal that the aggregates are large and multilayered, a larger value of n is recommended so that a larger number of cells may be incorporated into aggregates having larger projected areas. n should be set equal to 3/2 if the clumps are hemispherical in nature.

Experimental observations of aggregate morphology (made either with confocal microscopy or by changing the focal plane on a light microscope) should be used to select the appropriate formula for distributing the stacked cells. For example, confocal microscope pictures of Jurkat cell aggregates activated by mAb 33B6 revealed that the average aggregate was ~30 μm (~2.5 layers) high. Also, the extent of cell stacking seemed to be independent of the size of the aggregates. With these observations, we chose the exponent n of Eq. 7 equal to 1. When $n = 1$, the number of cells $N_{sf}(t)$ located above the focal plane (*i.e.*, stacked on other cells) is:

$$N_{sf}(t) = \left(\frac{A_f(t)}{S(t) - S_{<3}(t)}\right)\left(\frac{S_0 - S(t)}{a_1}\right). \quad (8)$$

The total are $S_{<3}(t)$ was compared by summing the projected areas of all objects for which $A_f(t)$ is smaller than $3a_1$. It was subtracted from $S(t)$ to calculate the total projected area of the multilayered aggregates. By combining Eqs. 3 and 7, the following expression gives the number of cells in each object with projects area $A_f(t)$:

$$N_f(t) = \begin{cases} \dfrac{A_f(t)}{a_1} & \text{if } A_f(t) \le 3a_1 \\ \dfrac{A_f(t)}{a_1} + \left(\dfrac{(A_f(t))^n}{\sum_{A_i(t)>3a_1} A_i(t)^n}\right)\left(\dfrac{S_0 - S(t)}{a_1}\right) & \text{if } A_f(t) > 3a_1. \end{cases} \quad (9)$$

Aggregate Size Distribution

After calculating the number of cells in each aggregate, the cumulative size distribution is obtained as described in our earlier communication (13). Figure 2a presents the aggregation data from an experiment where Jurkat cells

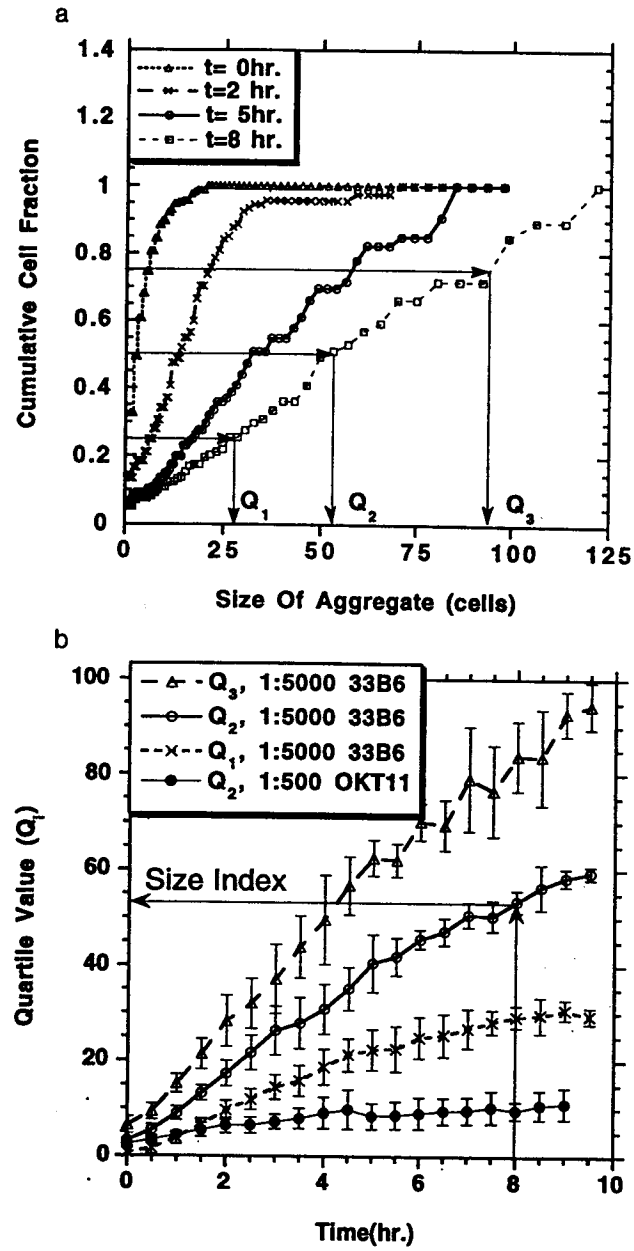

FIGURE 2. QUantifying aggregate size. (a) Jurkat cells seeded at a density of 1,700 cells mm^{-2} were activated with 33B6 at a dilution of 1:5,000, and the aggregate size distribution was monitored. The fraction of single cells decreases rapidly with time as larger aggregates are formed. Lines are smooth curves joining the peaks of the cumulative size distribution histograms. The figure also illustrates calculation of the quartile values (Q_1, Q_2, Q_3) at the 8-hr time point. These correspond to the size of aggregates below which 25, 50, and 75% of the cells are found. (b) Comparison of aggregate sizes for Jurkat cells treated with two antibodies. Jurkat cells incubated with 33B6 mAb (1:5,000 dilution) show extensive homotypic aggregation and their average aggregate size (Q_2) increases rapidly. Experiments with the OKT11 mAb (1:500 dilution) do not lead to formation of large aggregates. Data are shown as the mean ± SEM (n = 3).

were placed in wells of a 96-well tissue culture plate at a seeding density of 1,700 cells mm^{-2} and activated by adding 33B6 ascites at a dilution of 1:5,000. At the start of the experiment, most cells are nonaggregated, and only a small fraction of cells is incorporated into small aggregates. However, large aggregates are found on addition of 33B6, and very few cells have remained nonaggregated. Figure 2a is a cumulative size distribution showing the size distribution of cells at 0, 2, 5, and 8 hr after activation. The quartile values Q_1, Q_2, and Q_3 shown in this figure correspond to the aggregate size below which 25, 50, and 75% of the cells are found.

In the subsequent discussion, we will refer to the second quartile Q_2 of the cumulative size distribution as the *average aggregate size* $\hat{N}(t)$. The spread in the aggregate size distribution is quantified by

$$W = \frac{Q_3 - Q_1}{Q_2}. \qquad (10)$$

It is a useful parameter for (a) identifying subpopulations of cells that are nonadhesive in nature and (b) characterizing heterotypic aggregation. If some cells in a population are nonadhesive, for example, the Q_1 and Q_2 values will be small, compared with Q_3. Consequently, the spread in the aggregate size distribution will be larger than that obtained for cells with uniform adhesive properties.

The kinetics of the aggregation process can be followed by plotting the changes in the quartile values with time. The average aggregate size can be used as a measure to compare the aggregation kinetics under various treatments. Figure 2b shows the temporal evolution of the quartile values (Q_1, Q_2, and Q_3) for Jurkat cells on addition of 33B6 (1:5,000 dilution). The average aggregate size $\hat{N}(t)$ ($=Q_2$) of Jurkat cell aggregates on addition of 33B6 is compared with the experiment with mAb OKT11 (1:500 dilution). 33B6 stimulates vigorous homotypic aggregation, whereas the OKT11 mAb does not induce much intercellular aggregation. The standard errors for the experiment are small, compared with the changes of the average aggregate size. These and other results strongly indicate that we have developed a sensitive and reproducible assay for monitoring intercellular aggregation.

Aggregate Morphology Evolution

In our lymphocyte systems, cell stacking takes place because the strength of cell–cell bonds is stronger than the interaction between the cell and the tissue culture substrate. Consequently, the extent of stacking increases with increasing avidity between the cells. As noted previously, our assay quantifies changes in aggregate morphology by monitoring the decrease of the total projected area $S(t)$. As

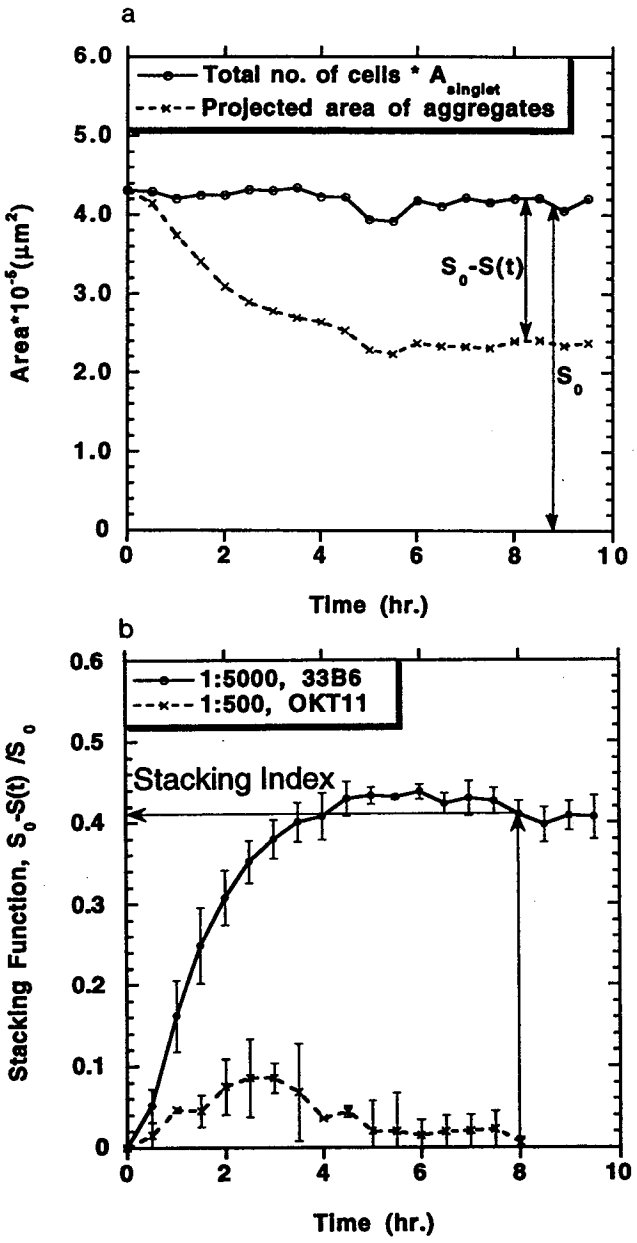

FIGURE 3. Quantifying aggregate morphology. (a) When Jurkat cells are activated with 33B6, the total projected area $S(t)$ of the cells and cell aggregates decreases from its initial values of S_0 (at $t = 0$) due to the formation of three-dimensional aggregates. However, the total number of cells remains virtually constant during an experiment. (b) Changes in aggregate morphology are quantified by the stacking function $h(t)$ defined as the fractional decrease of the total projected area of cells and aggregates during the course of the experiment. Addition of 33B6 ascites at a dilution of 1:5,000 to Jurkat cells leads to vigorous homotypic aggregation, whereas the control antibody 1:500 OKT11 does not result in cell stacking. Data shown are evaluated as mean ± SEM ($n = 3$).

shown in Fig. 3a for a typical experiment, the projected area $S(t)$ drops quickly below its initial value of S_0, due to the formation of three-dimensional aggregates. The relative decrease of $S(t)$, defined by the *stacking function*,

$$h(t) = \frac{S_0 - S(t)}{S_0}. \quad (11)$$

shows the temporal evolution of the extent of cell stacking. The stacking function quantifies the extent to which cells stack on top of each other to form three-dimensional clumps. Note that Fig. 3a also shows that the total number of cells and the computed S_0 remain fairly constant over the duration of the experiment, thus verifying the validity of the assumption we made in deriving this aggregation assay.

Figure 3b demonstrates the effect of cell activation on the morphology of the Jurkat cell aggregates on addition of 33B6 at a dilution of 1:5,000 and control mAb OKT11 at 1:500 dilution. On addition of 33B6, we observed a large and rapid decrease in the projected area, thus indicating the formation of large three-dimensional clumps. However, the morphology of cells on addition of OKT11 was relatively flat, and the stacking index was negligible 8 hr after start of the experiment. Although small three-dimensional aggregates were initially formed on addition of OKT11, they collapsed after 4 hr due to loss of cell avidity.

Aggregation Indices

Comparison of experimental aggregation data can be simplified by introducing two indices that summarize the pertinent information for each aggregation process. In Fig. 3b, on addition of 33B6, the stacking function $h(t)$ increased rapidly during the first few hours reaching a plateau after ~4 hr. Similarly, morphology of the aggregates formed when Jurkat cells were treated with mAb OKT11 at 1:500 dilution did not change appreciably after the first 4 hr. Similar experimental results were obtained for several lymphocyte aggregation systems showing that cell stacking takes place only during the first few hours of an experiment and that the ultimate morphology of the three-dimensional aggregates depends on treatment of the lymphocytes. The average aggregation size, however, continuously increases with time (Fig. 2b) as the motile aggregates continue to combine. Even a day after the start of an experiment, we continue to observe the formation of larger aggregates. Although the projected area of the larger aggregates continued to increase, however, the extent of vertical cell stacking remains virtually unchanged after the first few hours.

Based on these observations, we conclude that the extents of aggregation observed with different protocols can be evaluated by comparing both the average aggregated size and the aggregate morphology at some reference time that is sufficiently long for the stacking process to complete. In this study, the average aggregate size at the 8-hr time point is defined as the *size index, N**. The definition

TABLE 1. Size and stacking indices for Jurkat cells

Antibody	Antibody Dilution	Size Index (N^*)	Stacking Index (h^*)
33B6	1:5,000	54	0.41
OKT11	1:500	10	0.01

$$N^* = N(t = 8 \text{ hr}) \quad (12)$$

has worked well for out lymphocyte systems. Table 1 gives the values of the size index for the experiments presented in Fig. 2. Clearly, the Jurkat cells used herein aggregate very vigorously when we add 33B6 mAb at a dilution of 1:5,000 to the culture media.

The *stacking index h**, which describes the final extent of cell stacking, is defined as:

$$h^* = h(t = 8 \text{ hr}). \quad (13)$$

Table 1 shows the values of the stacking index for the two systems displayed in Fig. 3. The Jurkat/33B6 system exhibited large, three-dimensional aggregates 8 hr after activation, thus indicating high cell avidity. In contrast, the Jurkat/OKT11 system had small and flat aggregates (single cell layer).

CONCLUSIONS

This study has presented some significant improvements to our intercellular aggregation assay. The two indices that we introduced succinctly characterize both the extent of aggregation and the vertical stacking of the formed aggregates. In addition, the aggregation kinetics are accurately quantified with the two functions describing the temporal evolution of the average aggregate size and cell stacking. These indices and functions can be used to derive conclusions about cell avidity of cytoskeletal activity, and we have successfully used them to investigate the pathways of homotypic lymphocyte aggregation induced by mAbs to the β_1-integrin (14). A series of experiments (only a few of which were discussed herein) has shown that the developed assay is simple, sensitive, and has small reproducibility errors. Although we have developed this assay to study the kinetics of cellular aggregation processes, we believe it can also be applied to other biological and nonbiological agglutination systems.

REFERENCES

1. Arroyo, A. G., P. Sánchez-Mateos, M. R. Campanero, I. Martín-Padura, E. Dejana, and F. Sánchez-Madrid. Regulation of the VLA integrin-ligand interactions through the β_1 subunit. *J. Cell Biol.* 117:659–670, 1992.
2. Bednarczyk, J. L., and B. W. McIntyre. A monoclonal antibody to VLA-4 α-chain (CDw49d) induces homotypic lymphocyte aggregation. *J. Immunol.* 144:777–784, 1990.

3. Bednarczyk, J. L., J. N. Wygant, M. C. Szabo, L. Molinari-Storey, M. Renz, F. Fong, and B. W. McIntyre. Homotypic leukocyte aggregation triggered by a monoclonal antibody specific for a novel epitope expressed by the integrin β_1 subunit: conversion of nonresponsive cells by transfecting human integrin α_4 subunit cDNA. *J. Cell Biochem.* 51:465–478, 1993.
4. Born, G. V. R. Aggregation of blood by adenosine diphosphate and its reversal. *Nature* 194:927–929, 1962.
5. Campanero, M. R., A. G. Arroyo, R. Pulido, A. Ursa, M. S. de Matías, P. Sánchez-Mateos, P. D. Kassner, B. M. C. Chan, M. E. Hemler, A. L. Corbí, M. O. de Landázuri, and F. Sánchez-Madrid. Functional role of α2/β1 and α4/β1 integrins in leukocyte intercellular adhesion induced through the common β1 subunit. *Eur. J. Immunol.* 22:3111–3119, 1992.
6. Campanero, M. R., R. Pulido, M. A. Ursa, M. Rodríguez-Moya, M. O. de Landázuri, and F. Sánchez-Madrid. An alternative leukocyte homotypic adhesion mechanism, LFA-1/ICAM-1—independent, triggered th rough the human VLA-4 integrin. *J. Cell Biol.* 110:2157–2165, 1990.
7. Gonzalez, R. C., and R. E. Woods. Digital Image Processing. New York: Addison-Wesley Publication Company, 1992, pp. 299–302.
8. Hemler, M. E., M. J. Elices, C. Parker, and Y. Takada. Structure of the integrin VLA-4 and its cell-cell and cell-matrix adhesion functions. *Immunol. Rev.* 114:45–65, 1990.
9. Hynes, R. O. Integrins: versatility, modulation, and signaling in cell adhesion. *Cell* 69:11–25, 1992.
10. Konstantopoulos, K., K. K. Wu, M. M. Udden, E. I. Banez, S. J. Shattil, and J. D. Hellums. Flow cytometric studies of platelet responses to shear stress in whole blood. *Biorheology* 32:73–93, 1995.
11. Loeb, L. B. Kinetic Theory of Gases. New York: McGraw-Hill Book Company, Inc., 1927, pp. 29–40.
12. Moscona, A. Rotation-mediated histogenetic aggregation of dissociated cells: a quantifiable approach to cell interactions in vitro. *Exp. Cell Res.* 22:455–475, 1961.
13. Munn, L. L., M. W. Glacken, B. W. McIntyre, and K. Zygourakis. Analysis of lymphocyte aggregation using digital image analysis. *J. Immunol. Methods* 166:11–25, 1993.
14. Neelamegham, S., S. I. Simon, B. W. McIntyre, and K. Zygourakis. Induction of homotypic lymphocyte aggregation: evidence of a novel activation state of the β_1 integrin. *J. Leukoc. Biol.* 59:872–882, 1996.
15. O'Brien, J. R. Platelet aggregation. II. Some results with a new method of study. *J. Clin. Pathol.* 15:452–463, 1962.
16. Rothlein, R., and T. A. Springer. The requirement for lymphocyte function-associated antigen 1 in homotypic leukocyte adhesion stimulated by phorbol ester. *J. Exp. Med.* 163: 1132–1148, 1986.
17. Shimizu, Y., G. A. Van Seventer, K. J. Horgan, and S. Shaw. Roles of adhesion molecules in T-cell recognition: fundamental similarities between four integrins on resting human T cells (LFA-1, VLA-4, VLA-5, VLA-6) in expression, binding, and costimulation. *Immunol. Rev.* 114:109–143, 1990.
18. Simon, S. I., J. D. Chambers, and L. A. Sklar. Flow cytometric analysis and modeling of cell-cell adhesive interactions: the neutrophil as a model. *J. Cell Biol.* 111:2747–2756, 1990.
19. Steinkamp, J. A., M. J. Fulwyler, J. R. Coulter, R. D. Hiebert, J. L. Horney, and P. F. Mullaney. A new multiparameter separator for microscopic particles and biological cells. *Rev. Sci. Instr.* 44:1301–1310, 1973.
20. van de Wiel-van Kemenade, E., Y. van Kooyk, A. J. de Boer, R. J. F. Huijbens, P. Weder, W. van de Kasteele, C. J. M. Melief, and C. G. Figdor. Adhesion of T and B lymphocytes to extracellular matrix and endothelial cells can be regulated through the β subunit of VLA. *J. Cell Biol.* 117:461–470, 1992.

APPENDIX

Correction for Variations in Cell Seeding Density

Variations in cell seeding density among experiments will affect the number of cell–cell collisions and, thus, the computed values of average aggregate size. To account for such variations, we must correct the average aggregate size, $\hat{N}(t)$, calculated for an experiment starting with cell density c, by multiplying it with a normalization factor. This factor accounts for the variation in seeding density by normalizing the computed $\hat{N}(t)$ with respect to a reference seeding density c^*. If we denote the cell–cell collision frequency when the cell seeding density is c and c^* by Z and Z^*, respectively, then the corrected value of the average aggregate size is given by,

$$\hat{N}(t)_{\text{normalized}} = \hat{N}(t) \times \frac{Z^*}{Z}. \tag{A1}$$

In this assay, we assume that the normalization factor is independent of time and calculate it only once at the start of the experiment ($t = 0$). The normalization factor is derived using an analogy with the kinetic theory of gases. This theory predicts that the frequency of collisions between gas molecules moving in a three-dimensional control volume is

$$Z^{(3)} = \frac{\nu S^{(3)}}{4U^{(3)}}, \tag{A2}$$

where ν is the mean speed of the gaseous molecules, $S^{(3)}$ is the total area of the surface on which collisions can occur, and $U^{(3)}$ is the volume available for the molecule to move in (11). In our lymphocyte system, the cells migrate along the two-dimensional well surface with a certain velocity. To simplify our problem, we may consider the cells as circles with uniform diameter d moving on the planar substrate. When two cells collide, the distance between their centers is the cell diameter d. THus, there is a circle of radius d surrounding each cell that constitutes the area of exclusion, A_{ex}. When the center of any other cell comes in contact with this hypothetical circular surface, we have a cell–cell collision. If we modify Eq. A2 for our two-dimensional problem, we can easily show that the collision frequency $Z^{(2)}$ between cells is

$$Z^{(2)} \propto \frac{S^{(2)}}{U^{(2)}}, \tag{A3}$$

where $S^{(2)}$ is the perimeter along which collision can occur, and $U^{(2)}$ is the area available for the cell to move in. Equations A1 and A3 yield

$$\hat{N}(t)\text{normalized} = \hat{N}(t) \times \frac{S^*}{U^*} \times \frac{U^{(2)}}{S^{(2)}}, \tag{A4}$$

where S^* and U^* are the perimeter of collision and the area available for the cells to move in when the seeding cell seeding density is c^*. The collision frequency $S^{(2)}$ is proportional to the cell seeding density and can be expressed as

$$S^{(2)} = N_0 \times (2\pi d), \tag{A5}$$

where N_0 is the number of seed cells. The area $U^{(2)}$ is smaller than the monitored area of aggregation A_{img} by an amount b that one might set at first equal to the total area occupied by the N_0 circles of radius d. Actually, however, b is only one-half of this value because during the collision of a given cell, only half of its area is directed toward the relative motion of the approaching cell. Thus,

$$b = \frac{1}{2}A_{ex} = \frac{1}{2}(A_{img} - U^{(2)}) = \frac{1}{2}(\pi d^2 N_0). \tag{A6}$$

$\hat{N}(t)_{normalized}$ can now be computed by combining equations (A4 to A6). It is given by:

$$\hat{N}(t)_{normalized} = \hat{N}(t) \times \frac{c^*}{c} \times \frac{\left(A_{img} - \frac{1}{2}A_{ex}\right)}{\left(A_{img} - \frac{1}{2}A_{ex}^*\right)} \tag{A7}$$

where A_{ex} and A_{ex}* are the excluded areas at the actual and reference seeding densities, respectively. For our aggregation experiments with Jurkat cells, data are normalized to a reference cell seeding density of 1,700 cells mm^{-2}. Total area of the composite image A_{img} is 19.4×10^5 μm^2 (12×10^5 pixels), and the excluded area A_{ex}* of cells at the reference seeding density of 1,700 cells mm^{-2} is 8.6×10^5 μm^2 (because the average Jurkat cell has an area of 130.38 μm^2).

Our experiments have shown that stacking is not affected by cell seeding density. Thus, there is no need to correct the stacking function for variations in cell seeding density.

NOMENCLATURE

t = Time (sec)
j = Counter for objects (dimensionless)
M = Gray-level value corresponding to the minimum in the gray-level histogram (dimensionless)
T = Image segmentation gray-scale value (dimensionless)
K = A constant in the image segmentation equation (dimensionless)
$H(M)$, $H(T)$ = Gray-scale histogram function, frequency of pixels corresponding to M and T (dimensionless)
M_0 = Total number of objects identified at initial time (dimensionless)
$M(t)$ = Total number of objects identified at time t (dimensionless)
$A_j(t)$ = Projected area of the j^{th} object at time t (μm^2)
S_0 = Total initial projected area of all cells (μm^2)
$S(t)$ = Total projected area of cells and cell aggregates at time t (μm^2)
n = Exponent in the cell stacking assumption (dimensionless)
a_1 = Projected area of a single cell (μm^2)
N_0 = Initial number of cells in the experiment (cells)
$N_{bj}(t)$ = Number of cells located at the base of the three-dimensional aggregate in the j^{th} object (cells)
$N_{sj}(t)$ = Number of cells stacked on top of other cells in the j^{th} object and therefore not touching the plate surface (cells)
$N_s(t)$ = Total number of cells stacked on top of other cells (cells)
$S_{<3}(t)$ = Total projected area of aggregates with fewer than 4 cells (μm^2)
Q_1, Q_2, Q_3 = First, second, and third quartiles calculated from the cumulative size distribution (cells)
W = Spread of the aggregate size distribution (dimensionless)
$\hat{N}(t)$ = Average aggregate size, equals Q_2 (cells)
N^* = Size index, equals $\hat{N}(t)$ at 8 hr (cells)
$h(t)$ = Stacking function, used to quantify cell stacking (dimensionless)
h^* = Stacking index, equals $h(t)$ at 8 hr (dimensionless)
c = Experimental cell seeding density (cells mm^{-2})
c^* = Reference seeding density (cells mm^{-2})
Z^* = Collision frequency at reference seeding density (dimensionless)
$Z^{(3)}$ = Collision frequency between gaseous molecules in the three-dimensional space (dimensionless)
$Z^{(2)}$ = Collision frequency between lymphocytes

on the two-dimensional well surface (dimensionless)

$S^{(3)}$ = Total area of the surface on which collision can occur in three dimension equals surface area of all the gaseous molecules (μm^2)

$S^{(2)}$ = Perimeter on which collision can occur in two-dimensional well surface (μm)

S^* = Perimeter of collision at the reference cell seeding density (μm)

$U^{(3)}$ = Volume in three-dimensional space in which gaseous molecules can move (μm^3)

$U^{(2)}$ = Area on two-dimensional well surface on which cells can move (μm^2)

U^* = Area on well surface on which cells can move evaluated at the reference cell seeding density (μm^2)

v = Mean speed of gaseous molecule in three-dimensional space ($\mu m\ hr^{-1}$)

d = Diameter of Jurkat cell (μm)

A_{im} = Monitored area during experiment (μm^2)

A_{ex} = Total excluded area of the cells (μm^2)

A_{ex}^* = Total excluded area of the cells at the reference cell seeding density (μm^2)